Near-field photodetection with high spatial resolution by nanocrystal quantum dots

M. Hegg*, L. Y. Lin

Department of Electrical Engineering, University of Washington, Box 352500 Seattle, WA 98195-2500 USA
**Corresponding author: hegqm@u.washington.edu*

Abstract: We report a new demonstration of nanoscale solution-processed photodetectors by fabricating a nano-sized gap between two electrodes and drop-casting nanocrystal quantum dots (NCQDs) into the gap. We demonstrate a detection sensitivity of 62 pW with a max responsivity of 2.7 mA/W over a device with a nano-gap of 25 nm. Additionally, we characterize the dependence of signal-to-dark current ratio and responsivity on nano-gap size. Responsivity ranges from 1 – 90 mA/W for a nano-gap size range of 25 nm – 1.5 nm. Our results represent the first demonstration of how near-field optical detection for sub-diffraction nanophotonic integrated circuits can be achieved in principle using NCQDs.

OCIS codes: (040.0040) Detector; (040.5160) Photodetectors; (270.5570) Quantum detectors; (230.5590) Quantum-well, -wire and-dot devices

References and links

1. S. A. Maier, P. G. Kik, H. A. Atwater, S. Meltzer, E. Harel, B. E. Koel, and A. A. G. Requicha, "Local detection of electromagnetic energy transport below the diffraction limit in metal nanoparticle plasmon waveguides," Nature Materials **2**, 229-232 (2003).
2. S. A. Maier, P. E. Barclay, T. J. Johnson, M. D. Friedman, and O. Painter, "Low-loss fiber accessible plasmon waveguide for planar energy guiding and sensing," Appl. Phys. Lett. **84**, 3990-3992 (2004).
3. T. Yatsui, W. Nomura, and M. Ohtsu, "Self-assembly of size- and position-controlled ultralong nanodot chains using near-field optical desorption," Nano Lett. **5**, 2548-2551 (2005).
4. C. J. Barrelet, A. B. Greytak, and C. M. Lieber, "Nanowire photonic circuit elements," Nano Lett. **4**, 1981-1985 (2004).
5. E. Yablonovitch, "Photonic crystals - Towards rational material design," Nature Materials **2**, 648-649 (2003).
6. M. F. Yanik, S. H. Fan, M. Soljacic, and J. D. Joannopoulos, "All-optical transistor action with bistable switching in a photonic crystal cross-waveguide geometry," Opt. Lett. **28**, 2506-2508 (2003).
7. C. A. Barrios, V. R. Almeida, R. Panepucci, and M. Lipson, "Electrooptic modulation of silicon-on-insulator submicrometer-size waveguide devices," IEEE J. Lightwave Technol. **21**, 2332-2339 (2003).
8. M. Law, D. J. Sirbuly, J. C. Johnson, J. Goldberger, R. J. Saykally, and P. D. Yang, "Nanoribbon waveguides for subwavelength photonics integration," Science **305**, 1269-1273 (2004).
9. M. Ohtsu, K. Kobayashi, T. Kawazoe, S. Sangu, and T. Yatsui, "Nanophotonics: Design, fabrication, and operation of nanometric devices using optical near fields," IEEE J. Sel. Top. Quantum Electron. **8**, 839-862 (2002).
10. J. F. Wang, M. S. Gudiksen, X. F. Duan, Y. Cui, and C. M. Lieber, "Highly polarized photoluminescence and photodetection from single indium phosphide nanowires," Science **293**, 1455-1457 (2001).
11. O. Hayden, R. Agarwal, and C. M. Lieber, "Nanoscale avalanche photodiodes for highly sensitive and spatially resolved photon detection," Nature Materials **5**, 352-356 (2006).
12. M. Freitag, Y. Martin, J. A. Misewich, R. Martel, and P. H. Avouris, "Photoconductivity of single carbon nanotubes," Nano Lett. **3**, 1067-1071 (2003).
13. O. Astafiev, S. Komiyama, T. Kutsuwa, V. Antonov, Y. Kawaguchi, and K. Hirakawa, "Single-photon detector in the microwave range," Appl. Phys. Lett. **80**, 4250-4252 (2002).
14. J. Alda, J. M. Rico-Garcia, J. M. Lopez-Alonso, and G. Boreman, "Optical antennas for nano-photonic applications," Nanotechnology **16**, S230-S234 (2005).
15. K. T. Posani, V. Tripathi, S. Annamalai, N. R. Weisse-Bernstein, S. Krishna, R. Perahia, O. Crisafulli, and O. J. Painter, "Nanoscale quantum dot infrared sensors with photonic crystal cavity," Appl. Phys. Lett. **88**, 151104, (2006).
16. A. P. Alivisatos, "Semiconductor clusters, nanocrystals, and quantum dots," Science **271**, 933-937 (1996).
17. C. B. Murray, D. J. Norris, and M. G. Bawendi, "Synthesis and Characterization of Nearly Monodisperse Cde (e = S, Se, Te) Semiconductor Nanocrystallites," J. Am. Chem. Soc. **115**, 8706-8715 (1993).

#89377 - $15.00 USD Received 5 Nov 2007; revised 3 Dec 2007; accepted 4 Dec 2007; published 7 Dec 2007

18. G. M. Whitesides, J. P. Mathias, and C. T. Seto, "Molecular Self-Assembly and Nanochemistry - A Chemical Strategy for the Synthesis of Nanostructures," Science **254**, 1312-1319 (1991).
19. R. D. Schaller, M. Sykora, S. Jeong, and V. I. Klimov, "High-efficiency carrier multiplication and ultrafast charge separation in semiconductor nanocrystals studied via time-resolved photoluminescence," J. Phys. Chem. B **110**, 25332-25338 (2006).
20. R. D. Schaller, M. Sykora, J. M. Pietryga, and V. I. Klimov, "Seven excitons at a cost of one: Redefining the limits for conversion efficiency of photons into charge carriers," Nano Lett. **6**, 424-429 (2006).
21. E. J. Gansen, M. A. Rowe, M. B. Greene, D. Rosenberg, T. E. Harvey, M. Y. Su, R. H. Hadfield, S. W. Ham, and R. P. Mirin, "Photon-number-discriminating detection using a quantum-dot, optically gated, field-effect transistor," Nature Photonics **1**, 585-588 (2007).
22. M. Drndic, M. V. Jarosz, N. Y. Morgan, M. A. Kastner, and M. G. Bawendi, "Transport properties of annealed CdSe colloidal nanocrystal solids," J. Appl. Phys. **92**, 7498-7503 (2002).
23. N. Y. Morgan, C. A. Leatherdale, M. Drndic, M. V. Jarosz, M. A. Kastner, and M. Bawendi, "Electronic transport in films of colloidal CdSe nanocrystals," Phys. Rev. B **66**, 075339, (2002).
24. G. Konstantatos, I. Howard, A. Fischer, S. Hoogland, J. Clifford, E. Klem, L. Levina, and E. H. Sargent, "Ultrasensitive solution-cast quantum dot photodetectors," Nature **442**, 180-183 (2006).
25. G. Konstantatos, J. Clifford, L. Levina, and E. H. Sargent, "Sensitive solution-processed visible-wavelength photodetectors," Nature Photonics **1**, 531-534 (2007).
26. C. J. Wang, L. Huang, B. A. Parviz, and L. Y. Lin, "Subdiffraction photon guidance by quantum-dot cascades," Nano Lett. **6**, 2549-2553 (2006).
27. David Ginger and Neil Greenham, "Electrical Properties of Semiconductor Nanocrystals," in *Semiconductor and Metal Nanocrystals: Synthesis and Electronic and Optical Properties*, Victor I.Klimov, ed., (Marcel Dekker, Inc., New York, 2004), pp. 239-288.
28. H. C. Liu and G. C. Aers, "Resonant Tunneling Through One-Dimensional, Two-Dimensional, and 3-Dimensionally Confined Quantum Wells," J. Appl. Phys. **65**, 4908-4914 (1989).
29. A. K. Mahapatro, S. Ghosh, and D. B. Janes, "Nanometer scale electrode separation (nanogap) using electromigration at room temperature," IEEE Transactions on Nanotechnology **5**, 232-236 (2006).
30. A. K. Mahapatro, A. Scott, A. Manning, and D. B. Janes, "Gold surface with sub-nm roughness realized by evaporation on a molecular adhesion monolayer," Appl. Phys. Lett. **88**, 151917, (2006).
31. D. L. Klein, R. Roth, A. K. L. Lim, A. P. Alivisatos, and P. L. Mceuen, "A single-electron transistor made from a cadmium selenide nanocrystal," Nature **389**, 699-701 (1997).
32. L. Huang, M. C. Hegg, C.-J. Wang, and L. Y. Lin, "Fabrication of a nanophotonic waveguide and photodetector integrated device," Micro and Nano Letters (to be published)

1. Introduction

As the integration density of photonic integrated circuits progresses towards the sub-micron regime due to advanced optical waveguiding technologies such as plasmonics [1-3], nanowires and nanoribbons [4], photonic crystals [5,6], and high index silicon-on-insulators [7], it becomes imperative to detect the optical signal with nanometer resolution as well in order to preserve the on-chip integration density [4,8,9]. The requisite photodetection devices are critical for integration of nanophotonics with electronics. Previous approaches to near-field optical detection using nanostructures include single [10] and crossed-nanowire [11] devices, photosensitive carbon nanotubes [12], single-electron-transistors (SETs) [13], nano-antenna structures [14], and nanocrystal-enhanced photonic crystal structures [15]. These novel approaches, while advancing certain aspects of nanoscale photodetection, either do not provide the fabrication flexibility and convenient materials necessary for nanophotonic integrated circuit design or have large overall device sizes. An alternative approach is to use colloidal nanocrystal quantum dots as the building blocks for nanophotonic integrated circuits. Colloidal NCQDs have unique optoelectronic properties such as sharp absorption, emission and gain bands. They have nano-scale dimensions and the emission and absorption wavelength can be tuned simply by changing their size [16,17]. They have flexible surface chemistry that can be modified for various self-assembly fabrication, which provides a powerful route to integrated fabrication [18]. Furthermore, carrier multiplication (CM) has been shown to be highly efficient in NCQDs due to confinement-enhanced Coulomb coupling between single-and multi-exciton states, which is a unique feature of semiconductor nanocrystals [19]. Internal quantum efficiencies as high as 700% have been experimentally demonstrated [20], suggesting the possibility for ultra-high sensitivity photodetection. Photon counting has been demonstrated by an epitaxially-grown QD field-effect transistor over a dark

#89377 - $15.00 USD Received 5 Nov 2007; revised 3 Dec 2007; accepted 4 Dec 2007; published 7 Dec 2007

current floor of 80 pA [21]. Thin films of CdSe NCQDs have been shown to exhibit remarkable photoconductive properties, making them ideally suited for photodetector-based applications [22,23]. Indeed, large-area, solution-processed CdSe NCQD photodetectors have demonstrated high sensitivity while being relatively straightforward to fabricate [24,25]. Here, we present an approach to near-field optical detection that combines solution-processing with nanoscale device size, improving on the spatial resolution, fabrication flexibility, integration density, and sensitivity of previous work. We have previously demonstrated the utility of NCQDs for nanophotonic applications by fabricating sub-diffraction quantum dot (QD) cascade waveguides for high-density on-chip interconnection [26]. The nano-scale photodetector reported here provides a detection approach that can be readily integrated with the QD waveguides without compromising the interconnection density.

Electron transport in NCQDs embedded in an *n-i-n* (metal-QD-metal) structure typically involves significant potential barriers at the QD-QD interface as well as the QD-Electrode interface. Transport between NCs can, therefore, be considered as a problem of hopping between localized states [27], and can be modeled by the transfer Hamiltonian approach [28]. Carriers with higher energies have a higher probability of tunneling through the QDs and contributing to the tunneling current. The effect of optical excitation on the electrical transport of such structures is thus to reduce the effective potential barrier from the QD to the electrode by exciting photo-generated carriers into higher energy states. Fig. 1(a) shows an energy diagram for a NCQD in the absence of light. Γ_{1D} is the tunneling rate out of the NCQD for a carrier that has accessed the ground state of the conduction band via thermal energy, weak optical excitation, or tunneling from the source (Γ_{1S}). Fig. 1(b) is the NCQD in the presence of light. Γ_2 is the tunneling rate for a carrier promoted to a higher energy level under strong optical excitation, and $\Gamma_2 > \Gamma_1$. Fig. 1(c) shows qualitative current (I)-voltage (V) characteristics for the ideal case at low temperatures. The I-V characteristics should exhibit strong resonant behavior, corresponding to overlap between the top of the Fermi sea in the metal electrodes and the δ-function-like energy states. At room temperatures, this resonance will be difficult to observe due to homogeneous and inhomogeneous linewidth broadening of the energy states in the QDs. As our ultimate goal is to build a device for nanophotonic integrated circuit applications under regular environmental conditions, we focus our experimental study on measurements at room temperature.

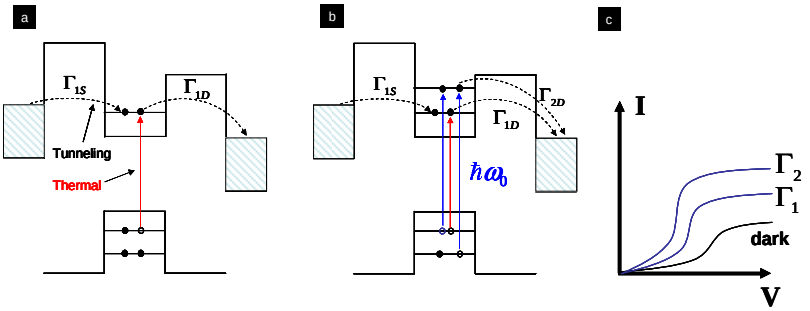

Fig. 1. Energy diagram of NCQD **a,** in the absence of light **b,** in the presence of light. $\hbar\omega_0$ is the photon energy which promotes an electron from the valence to conduction band, Γ is the tunneling rate for a carrier in the conduction band of the NCQD, and $\Gamma_1 < \Gamma_2$. **c,** Schematic I-V characteristics of a nano-scale NCQD photodetector.

2. Fabrication

Figure 2 shows a schematic of the fabrication steps involved in constructing a nano-scale quantum dot photodetector. A Si wafer with a 1 μm surface layer of SiO_2 is used as the substrate. The wafer is spin-coated with a 100 nm layer of polymethyl methacrylate (PMMA) photoresist and patterned by electron-beam lithography (EBL) to make narrow continuous electrode patterns with line widths of 50 nm connected to large-area contact pads of 50×50

#89377 - $15.00 USD Received 5 Nov 2007; revised 3 Dec 2007; accepted 4 Dec 2007; published 7 Dec 2007

μm. After developing the PMMA, the exposed SiO_2 is silanized with a monolayer of (3-Mercaptopropyl)trimethoxysilane (MPTMS). To perform silanization, the wafer is oxygen-plasma cleaned and then exposed to the MPTMS gaseous molecules inside a vacuum dessicator for two hours. The sample is then immediately transferred to a thermal evaporator for deposition of a 300-Å Au layer, followed by lift-off of PMMA to form the Au electrodes. The electrodes are broken to form a nano-gap by continuously increasing a voltage across the electrodes at a rate of 0.1 mV/sec. After the onset of electromigration [29], the conductance is monitored until a deviation by 90% from the original conductance is observed, at which point the applied bias is turned off. After confirmation of the break using scanning electron microscopy (SEM), a 100 μM solution of CdSe/ZnS NCQDs in toluene is drop-cast onto the wafer. The NCQDs have a nominal diameter (core + shell) of 5.2 nm, an emission wavelength of 620 nm, and are capped with trioctylphosphine oxide (TOPO) to passivate surface trap states and reduce nanocrystal aggregation.

The SiO_2 layer insulates the device from photo-generated carriers in the Si. The MPTMS monolayer acts as an insulating adhesion layer for the Au film [30]. I-V measurements show that MPTMS works better as the adhesion layer than regular metal such as Cr or Ti during the break-junction process, as regular metal often leaves a conduction trace and results in high dark current (~10's of nA compared to less than 1 pA using MPTMS). We use a drop-casting method to deposit the QDs between electrodes. This method results in a thin film of QDs over a large area, but only QDs in and around the nano-gap can contribute significantly to conduction (to be discussed in Sec. 4). A more location-specific deposition of the QDs can be achieved using thiol molecule self-assembly, which would bind the QDs to Au only [31], although such a process will result in large distances between the QDs and low tunneling currents when the gap between the electrodes is larger.

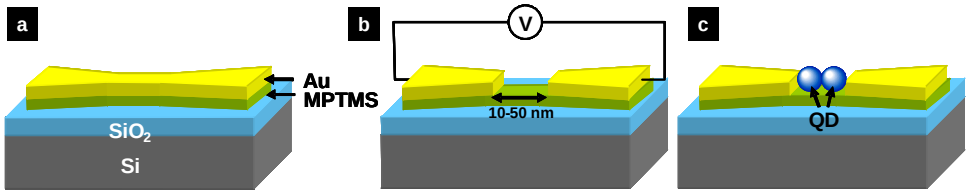

Fig. 2. Fabrication process of the NCQD photodetector. **a**, EBL and Au deposition with MPTMS as the adhesion layer. **b**, creating a nano-gap by break-junction procedure, and **c**, drop-casting QD deposition.

Electrodes having widths of 50 nm were broken with gap sizes ranging from 1.5 - 25 nm, in order to demonstrate the flexibility of the break-junction procedure. Figure 3(a) shows a large-area device structure and the magnified nano-gap region, revealing a narrow break-junction with 25 nm gap size. The large 100×150 μm contact pads are for probe-testing purpose only and are not an essential part of the active device. The break-junction process was chosen to achieve proof-of-concept demonstration of the device, but it requires breaking the electrodes in series. In principle, high-resolution EBL can also be used to pattern the nano-gap electrodes and eliminate the break-junction step [32]. Figure 3(b) shows an example of a device after drop-casting NCQDs into the nano-gap. The NCQDs fill the gap and the surrounding area of the device. Although QDs are deposited in a large area, only tunneling in and around the narrow break-junction gap can contribute significantly to the measured current.

#89377 - $15.00 USD Received 5 Nov 2007; revised 3 Dec 2007; accepted 4 Dec 2007; published 7 Dec 2007

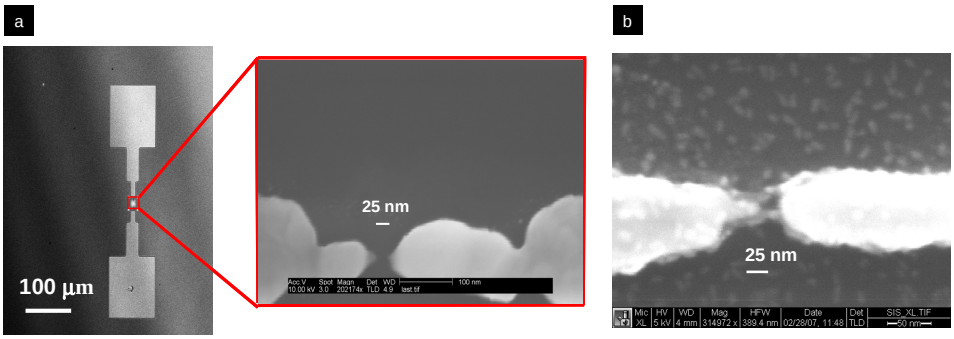

Fig. 3. Fabrication results. **a**, Scanning electron micrograph (SEM) of a pre-QD deposition break-junction electrode. **b**, SEM of a NCQD photodetector.

3. Results

Figure 4(a) shows control measurements performed on the 25 nm gap device shown in Fig. 3(a) prior to quantum dot deposition. I-V measurements with and without optical excitation were performed in order to demonstrate the nano-gap insensitivity to incident radiation. The results show that the measured tunneling current, either under illumination or dark condition, is less than 1 pA without the QDs throughout a bias range of 0-5V. The same measurement is then repeated for the device after NCQD deposition. Figure 4(b) shows the I-V characteristics of the device under illumination and dark conditions. The illumination intensity is 1 pW/nm^2. The tunneling current under dark conditions increases after the QDs are attached but still remains below 4 pA, confirming the placement of QDs between the electrodes. The photocurrent at 4 V is over 3 times larger than the dark current, confirming photosensitivity of the device. The specific contact resistance is the reciprocal of the slope of the dark current I-V curve at zero bias multiplied by the device cross-sectional area, and is calculated to be R_c = 16 Ωcm^2. The linearity of the dark current I-V curve and the low value for R_c indicate good ohmic contacts.

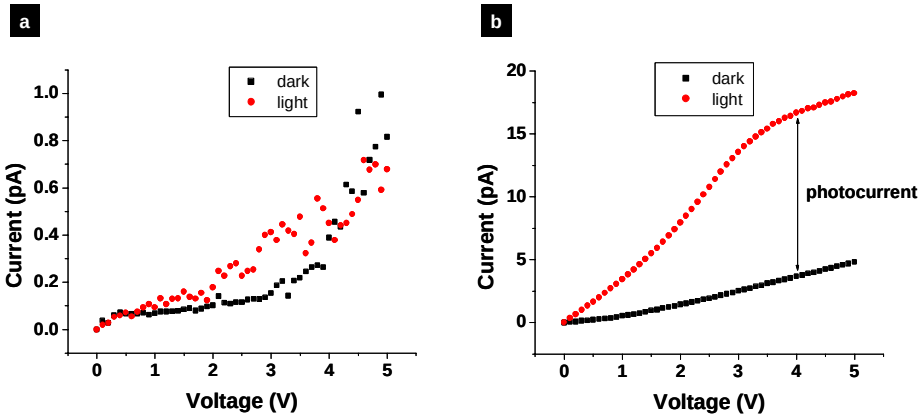

Fig. 4. Characterization of NCQD photodetectors. **a**, I-V characteristics of the break-junction electrode in dark (squares) and illuminated (circles) conditions. **b**, I-V characteristics of the NCQD photodetector under dark (squares) and illuminated (circles) conditions.

To properly calculate a device responsivity, an effective device area was estimated by simulating the electric field intensity in and around the nanogap. Fig. 5(a) shows a surface plot of the E-field intensity in and around a 20 nm nano-gap. The E-field is highest around the edges of the gap and decreases radially outward from the center. Fig. 5(b) shows how the E-field intensity decays rapidly with radial distance from the gap edges. For a 20 nm gap, E/E_{max} is approximately 10% when r = 50 nm. The photocurrent is a function of electric field,

#89377 - $15.00 USD Received 5 Nov 2007; revised 3 Dec 2007; accepted 4 Dec 2007; published 7 Dec 2007

number of QDs, and number of tunneling barriers between QDs. The electrode-to-electrode distance increases abruptly from < 30 nm to > 10 μm outside the nano-gap region. Although the total number of QDs increases, the distance between electrodes and the number of tunneling barriers both increase proportionally, which contribute negatively to the photocurrent. We therefore define the effective area of the device as the rectangular area of the nano-gap plus a circular area w/radius r defined by the distance from the electrode edge at which the E-field is 10% of the highest value. This distance scales linearly with gap size.

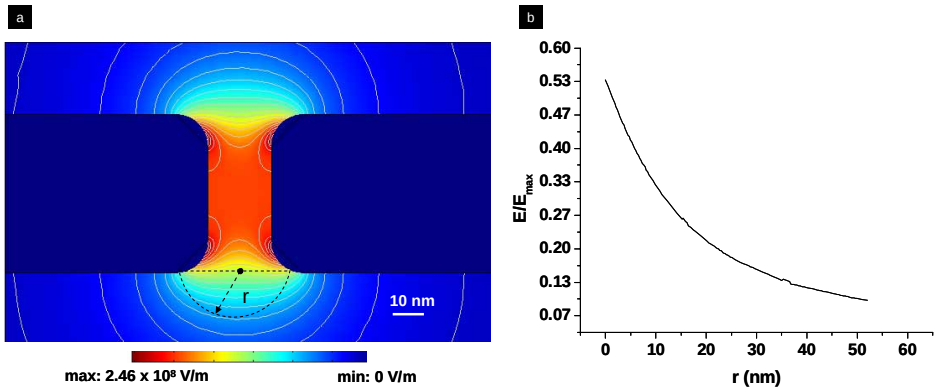

Fig. 5. Finite element simulation of the electric field in and around a 20nm nano-gap. **a**, Surface plot of the electric field intensity in and around the nano-gap. **b**, Plot of E/E_{max} vs. radial distance from the electrode edge.

To characterize the sensitivity and responsivity of the device, photocurrent measurements were performed under various illumination intensities, with the device biased at 4 V. Optical signal used for excitation is from a 405 nm laser source coupled to the device through a lensed fiber probe and focused to a spot size diameter of 100 μm. Current is measured using a Keithley 6430 sub-femtoamp source meter and the device is electrically shielded on a low-noise Cascade Microtech probe station. The results are shown in figure 6(a). The device starts to show measurable photocurrent of 80 fA under 62 pW illumination over the effective device area. No special shielding of ambient light was done for this measurement. The device has an average responsivity of 2.7 mA/W under low-intensity illumination, and starts to exhibit saturation effects when the optical power increases beyond 4 nW. The noise effective power (NEP) is the noise current divided by the responsivity under the same experimental conditions. From prior research of large devices with 5 um electrode spacing [24], the noise floor for 10 nA of dark current is approximately 0.1 $pA/Hz^{1/2}$. The device shown in Figure 4 exhibits 3.67 pA of dark current at 4V bias with a corresponding responsivity of 2.7 mA/W. If a noise floor of 0.1 $pA/Hz^{1/2}$ is used, this equates to an NEP of $3.7x10^{-11}$ $W/Hz^{1/2}$. This is effectively a lower bound for the NEP of our device. As an upper bound, if our device is shot noise-limited, the noise floor for 3.67 pA is $(2qI_dB)^{1/2}$ = 1.08 $fA/Hz^{1/2}$ which equates to an NEP of $4.01x10^{-13}$ $W/Hz^{1/2}$.

Several devices with a range of gap sizes from 1.5 – 25 nm were fabricated and tested. Figure 6(b) shows the signal-to-dark current ratio (SDR) and responsivity (R) of these devices as a function of gap size. The largest measured SDR is 3.5 for a gap of 25 nm and decreases with smaller gap size due to an increase in the dark current as the number of tunneling barriers between the electrodes is reduced. The largest device responsivity is nearly 0.1 A/W over the effective device area for a gap size of 1.5 nm and decreases with increasing gap size. This is because the absorbed optical power increases linearly with the gap size, but the tunneling photocurrent does not.

#89377 - $15.00 USD Received 5 Nov 2007; revised 3 Dec 2007; accepted 4 Dec 2007; published 7 Dec 2007

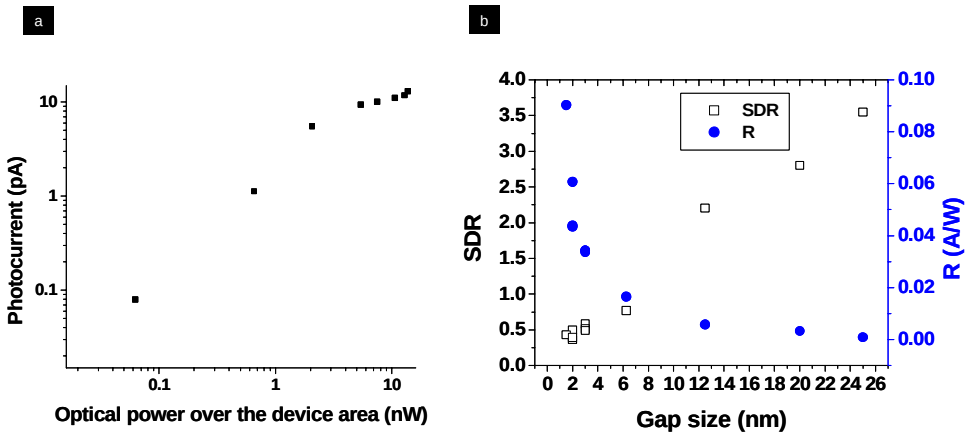

Fig. 6. Characterization results of the NCQD photodetector. **a**, Responsivity measured at room temperature using a calibrated 405 nm laser and biased at 4.0 V. **b**, Signal-to-dark current ratio SDR (squares) and responsivity R (circles) at 4V bias for devices of variable gap sizes.

Integrated fabrication of the QD waveguides and the QD photodetector has been demonstrated [32]. Figure 7 shows the SEM of the integrated device as the first step towards high-density photonic integrated circuits.

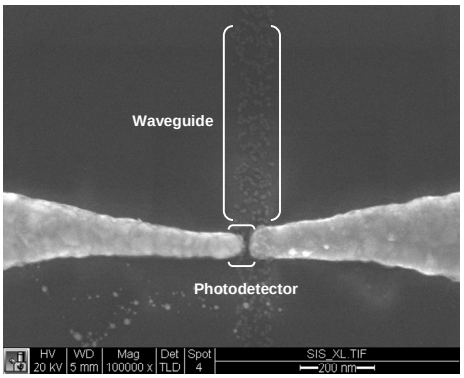

Fig. 7. Integrated photodetector and waveguide device.

4. Conclusion

In conclusion, we present the design, fabrication, and characterization results of a new nano-scale quantum dot photodetector. The device consists of QDs positioned by drop-casting into a nano-gap between two closely spaced electrodes. The gap is fabricated using a break-junction technique. The device improves the sensitivity level over previous nanoscale near-field photodetectors and is able to detect optical power as low as 62 pW with dark current less than 4 pA under normal environment. The spatial resolution of the device is limited only by the effective area of the photodetector and here we demonstrate spatial resolution as low as 120 nm^2 for the device with 1.5 nm gap and up to 13515 nm^2 for the device with 25 nm gap. Drop-casting NCQDs onto the electrodes demonstrates a simple and flexible fabrication technique that can be easily integrated with other self-assembled and solution-processed components of nanophotonic integrated circuits. Signal-to-dark current ratio and responsivity are characterized for devices with various gap sizes. The signal-to-dark current ratio increases linearly with gap-size due to a reduction of dark current with increasing tunneling length. The

#89377 - $15.00 USD Received 5 Nov 2007; revised 3 Dec 2007; accepted 4 Dec 2007; published 7 Dec 2007

responsivity is largest for small device area, due to the different dependence on gap size between the input optical power and the tunneling photocurrent. The characterization results provide a reference for nano-scale QD photodetector design. The nano-scale size, high sensitivity, and simple fabrication of the NCQD photodetector suggest a possible approach to integration of nanophotonics with electronics and detection of near-field on-chip optical signals.

Acknowledgments

We thank L. Huang for the SEM images shown in figure 3(b) and figure 7. M.C.H. thanks the NSF IGERT Graduate Fellowship Program and University of Washington UIF Graduate Fellowship Program for financial support. Work was performed in part at the University of Washington Nanotech User Facility (NTUF), a member of the National Nanotechnology Infrastructure Network (NNIN), which is supported by the National Science Foundation.

#89377 - $15.00 USD Received 5 Nov 2007; revised 3 Dec 2007; accepted 4 Dec 2007; published 7 Dec 2007